Foluso Ladeinde
Professor.

Wei Liu
Researcher.

Edward E. O'Brien
Professor.

Department of Mechanical Engineering,
SUNY at Stony Brook,
Stony Brook, NY 11794-2300

Turbulence in Compressible Mixing Layers

The direct numerical simulation (DNS) of two-dimensional compressible turbulent mixing layers is reported in this paper for convective Mach numbers M_c = 0.5, 0.8 and 1.0. All scales of flow are resolved with a 256^2 grid, although results are also obtained for 64^2, 96^2 and 128^2 grids for the purpose of determining the effective accuracy and grid-independence of our calculations. The effect of Mach number is also reported for all the Reynolds stress tensor components and for the "shear" components of the anisotropy tensor, the dissipation tensor, pressure-strain, and the triple correlation tensor. The short-time behaviors of some of these quantities are similar to those reported by Sarkar (1995) for homogeneous shear flow, in spite of the differences in the problem type and initial and boundary conditions. The relative magnitudes and signs of the unclosed terms in the Reynolds stress equations provide information on those that have to be retained for turbulence modeling as well as the sense of their contribution.

1 Introduction

Turbulence mixing layers represent a prototype of the mixing that takes place during combustion in some propulsion systems. Because this phenomenon occurs at high speed, the effect of compressibility has been studied (Sandham and Reynolds, 1991). The reference just cited also contains much of the relevant fluid dynamical work on compressible mixing layers, to which the reader should refer.

The goal in our work is to acquire a detailed understanding of compressible mixing layers with an emphasis on results that may eventually lead to affordable Reynolds stress models for engineering calculations (see Ladeinde, 1995). Therefore, a significant portion of this paper is devoted to investigation of the intensity of second moment terms in the evolution equations for the Reynolds stress tensor, with a particular emphasis on the unclosed terms in the equations. Previous work on compressible mixing layers does not address this issue.

The results reported in this paper are based on the direct numerical simulation of compressible turbulence. The numerical procedures and the validation of our computer program will be presented, together with the results on the magnitudes of some of the second moments and the effect of Mach number.

2 Mathematical Formulation

The pertinent equations are those that govern the conservation of mass, momentum and thermodynamic energy under compressible conditions. Further, each nondimensional variable is decomposed as follows, taking velocity u_i as an example:

$$u_i = \bar{u}_i + u_i'.$$

Here, an overline represents a Reynolds-averaged quantity whereas a superscripted prime denotes fluctuations. The governing equations are solved in the nondimensional form, with the free-stream velocity $\bar{u}_\infty = \bar{u}|_{y\to\infty}$ taken as the velocity scale and the vorticity thickness δ_ω as length scale, which is defined as

$$\delta_\omega = \frac{\Delta U_\infty}{\left|\dfrac{d(\overline{\rho u}/\bar{\rho})}{dy}\right|_{y=0}},$$

where ΔU_∞ is the velocity difference across the layer, i.e., $\Delta U_\infty = \bar{u}|_{y\to\infty} - \bar{u}|_{y\to-\infty}$. The mean velocity profile in all cases is given by:

$$\bar{u} = \tanh(2y).$$

The initial mean temperature profile is calculated using the Crocco-Busemann relation, and assuming unity Prandtl number:

$$\bar{T} = 1 + M_c^2 \frac{(\gamma - 1)}{2}(1 - \bar{u}^2),$$

where γ is the ratio of specific heats and M_c is the free-stream Mach number (or convective Mach number), defined as

$$M_c = \frac{\Delta U_\infty}{c_\infty}.$$

The quantity c_∞ is the free-stream sound speed. Uniform pressure is assumed for the initial mean flow ($\bar{p}_0 = 1$) and the mean density profile is obtained from:

$$\bar{\rho}_0 = \frac{\bar{\rho}_0 \bar{T}_0}{\gamma M_c^2}.$$

Superimposed on the mean velocity profile are disturbances of the form

$$u' = A_m \frac{yL}{10\pi} \sin\left(\frac{2\pi x}{L_x}\right) e^{-(y^2/10)}, \tag{1}$$

$$v' = A_m \cos\left(\frac{2\pi x}{L_x}\right) e^{-(y^2/10)}, \tag{2}$$

where the amplitude A_m is chosen to be 0.05, following Sandham and Yee (1989) and L_x is the length of the domain in x-direction. The computational domain is $(x, y) \in (0, 20) \times (-50, 50)$. The velocity perturbation in the y-direction is made to resemble the eigenfunction from the linear theory, while that for the streamwise component is chosen so that the entire disturbance is divergence-free.

Four different meshes, 64^2, 96^2, 128^2 and 256^2, are chosen for our calculations. For each mesh, a constant grid size distribution is employed in the streamwise direction, i.e., constant Δx, while, in the cross stream, the grid points are unequally spaced, with mesh concentration near the center of the layer ($y = 0$), to cover the region dominated by large scale structures. The mesh generation routine is described in detail by Drummond

Contributed by the Fluids Engineering Division for publication in the JOURNAL OF FLUIDS ENGINEERING. Manuscript received by the Fluids Engineering Division November 21, 1996; revised manuscript received October 15, 1997. Associate Technical Editor: M. M. Sindir.

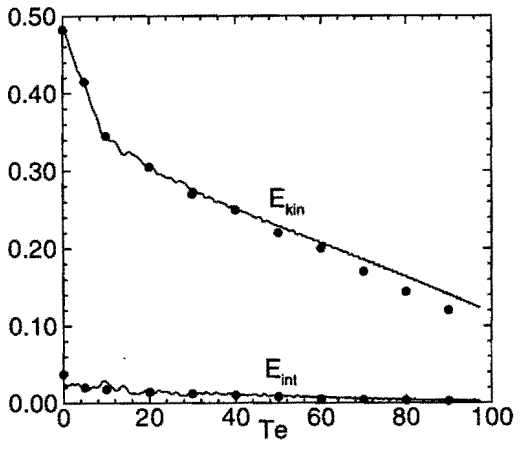

Fig. 1 Characteristics of the SV/PS (M_s = 0.5) Simulation. Results from our work (lines) are compared with the pseudospectral calculations by Ghosh and Matthaeus (1992) (dots). E_{kin} is total kinetic energy, E_{int} is total internal energy and T_e is eddy turn over time.

(1988). A periodic boundary condition is imposed in the x-direction. For the y-boundaries, a zero velocity gradient condition is imposed as a simpler but an acceptable alternative to the NSCBC conditions (Poinsot and Lele, 1992).

Each term of the evolution equations for the Reynolds stress tensor $\overline{\rho u_i'' u_j''}$ has been computed for the purpose of examining the intensity of turbulence in mixing layers. The goal here is to investigate the magnitudes of the unclosed terms in the equations and guide the modeling of these terms. The exact transport equation for the Reynold stress tensor is (Sarkar et al., 1991)

$$\underbrace{\frac{\partial}{\partial t}(\overline{\rho u_i'' u_j''})}_{1} + \underbrace{\frac{\partial}{\partial x_k}(\overline{\rho u_i'' u_j'' \tilde{u}_k})}_{2}$$

$$= \underbrace{\mathbf{P}_{ij}}_{3} + \underbrace{\pi_{ij}}_{4} - \underbrace{\mathbf{T}_{ijk,k}}_{5} - \underbrace{\overline{\rho}\epsilon_{ij}}_{6} + \underbrace{\frac{2}{3}\overline{p'\theta}\delta_{ij}}_{7}$$

$$+ \underbrace{(-u_i''\overline{p}_{,j} - \overline{u_j''}\overline{p}_{,i})}_{\text{Remaining Term1}} + \underbrace{(\overline{u_i''}\overline{\sigma}_{jk,k} + \overline{u_j''}\overline{\sigma}_{ik,k})}_{\text{Remaining Term2}}, \quad (3)$$

where

$$\mathbf{P}_{ij} = -\overline{\rho}(\widetilde{u_i'' u_k''}\tilde{u}_{j,k} + \widetilde{u_j'' u_k''}\tilde{u}_{i,k}),$$

$$\pi_{ij} = \overline{p' u_{i,j}'} + \overline{p' u_{j,i}'} - \tfrac{2}{3}\overline{p'\theta}\delta_{ij},$$

$$\mathbf{T}_{ijk} = \overline{\rho u_i'' u_j'' u_k''} + (\overline{p' u_i'}\delta_{jk} + \overline{p' u_j'}\delta_{ik}) - (\overline{u_i'\sigma_{jk}'} + \overline{u_j'\sigma_{ik}'}),$$

$$\overline{\rho}\epsilon_{ij} = \overline{\sigma_{ik}' u_{j,k}'} + \overline{\sigma_{jk}' u_{i,k}'},$$

$$\theta = u_{k,k}',$$

σ_{ij} is the viscous stress:

$$\sigma_{ij} = \mu(u_{i,j} + u_{j,i} - \tfrac{2}{3}u_{k,k}\delta_{ij}).$$

In Eq. (3), $\mathbf{P}_{ij}$ is the production, π_{ij} the deviatoric part of the pressure-strain correlation, $\mathbf{T}_{ijk}$ the diffusive transport, ϵ_{ij} the turbulent dissipation rate tensor and $\overline{p'\theta}$ the pressure-dilatation correlation. The symbol tilde, "~", on a variable indicates Favre-averaging defined, for any variable ϕ, as

$$\tilde{\phi} = \frac{\overline{\rho\phi}}{\overline{\rho}}.$$

All terms are calculated at position $y = 0$ at different times. In a modeling framework, the terms [4] to [7], Remaining Term1 and Remaining Term2 in (3) are unclosed and therefore need to be modeled.

3 Numerical Method

A high-order finite difference-based ENO (Essentially Non-Oscillatory) scheme is used for the direct numerical simulation (DNS) of compressible turbulence, details of which are available in Ladeinde et al. (1996). The procedure can be expressed in the operational form:

$$u(x_j, t_{n+1}) = E(\tau)\cdot R(\hat{f}(u(x_j, t_n)); \tau), \quad (4)$$

where $E(\cdot)$ is an operator representing the advancement of the solution in time from level n to $n+1$, $\tau = t_{n+1} - t_n$ and $R(\cdot)$ is the reconstruction of the numerical flux, $\hat{f}$, which is of the form:

$$\hat{f}_{j+1/2}(u(x_j, t_n); \tau) = \sum_{k=0}^{md} c(i-j, k)\cdot f[i, k], \quad (5)$$

where md is the order of the procedure, c is a high-order interpolation coefficient, i is the left most point in the stencil used to approximate $\hat{f}_{j+(1/2)}$, and $f[i, k]$ is the undivided difference of the flux term.

A third-order explicit Runge-Kutta TVD scheme is used for the time advancement of the operator $E(\cdot)$ in Eq. (4). The primary dependent variables (ρ, u, v, E) were obtained directly from the ENO simulation. The pressures and temperatures were calculated as follows

$$p = (\gamma - 1)[E - \tfrac{1}{2}\rho(u^2 + v^2 + w^2)],$$

$$T = \frac{\gamma M_c^2 p}{\rho}.$$

4 Results

The computer program used for the present simulations has been validated for the kinds of calculations reported here. One of the validation exercises is reported in Ladeinde et al. (1995) and pertains to the DNS of the two-dimensional compressible turbulence problem investigated by Ghosh and Matthaeus (1992), who used the pseudospectral method. Four types of initial conditions were investigated. Figures 1 and 2 show the comparisons for the SV/PS initial condition case at M_s = 0.5 (see Ladeinde et al., 1995 for notations and details). In Fig. 1,

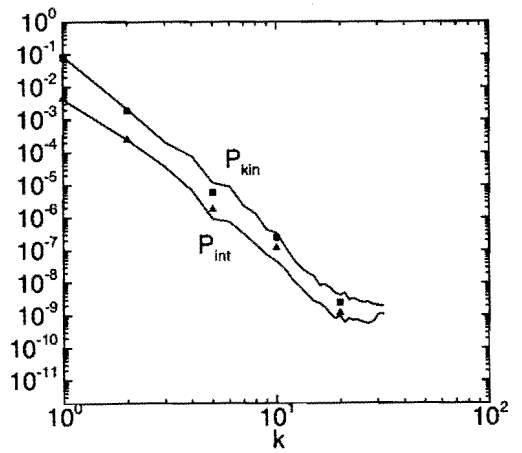

Fig. 2 Characteristics of the SV/PS (M_s = 0.5) Simulation. Results from our work (lines) are compared with the pseudospectral calculations by Ghosh and Matthaeus (1992) at $T_e \cong 20.5$. The circular and triangular symbols denote the results for of Ghosh and Matthaeus for P_{kin} and P_{int}, respectively. P_{kin} is kinetic energy spectrum, P_{int} is internal energy spectrum and T_e is eddy turn over time, and k is wavenumber.

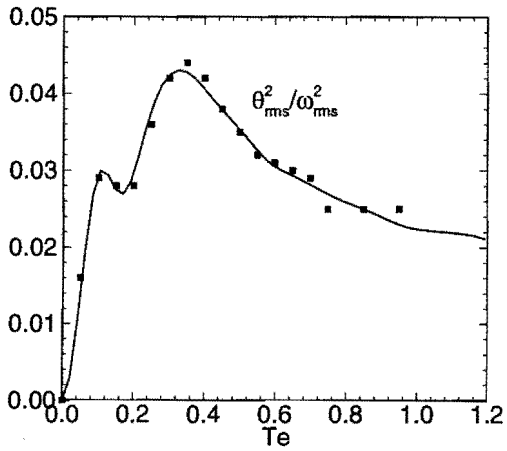

Fig. 3 Comparison of $\theta^2_{rms}/\omega^2_{rms}$ with the results in Lee et al. (1991) for eddy shocklets in three-dimensional decaying compressible turbulence. θ and ω are fluctuating dilatation and vorticity, respectively. Mach numbers, Ma, of 0.65 and 1.65 were compared, with comparable agreement. Figure shows the comparison for Ma = 0.65. T_e is eddy turn over time.

the time evolution of E_{int} (average internal energy) and E_{kin} (average kinetic energy) are shown. Figure 2 shows the spectra of the internal energy and the kinetic energy, as functions of the wavenumber. The excellent agreement between the two sets of calculations is apparent.

Another test to which our program was subjected consists of the reproduction of the results presented by Lee et al. (1991) for the eddy shocklets in decaying compressible turbulence. The conditions in Lee et al. were used except for the numerical procedure which, in Lee et al., is based on the compact Padé approximant scheme. Figures 3 shows the comparison of the ratio $\theta_{rms}/\omega_{rms}$ (where θ is fluctuating dilatation and ω is fluctuating vorticity) with the results reported by Lee et al. Good agreement is apparent. Comparisons were also made for the skewness and flatness (not shown), also with good agreement.

The simulation of the two-dimensional compressible turbulent mixing layers, on which our study of the turbulence moment equations is based, uses the same conditions as in Sandham and Yee (1989). Figure 4 shows the evolution of vorticity thickness δ_ω at M_c = 0.8, Re = 400 for different meshes. The same quantity calculated by Sandham and Yee with the TVD method and the McCormack method is also shown in Fig. 4 for comparison purposes. The vorticity, density, and pressure fields are

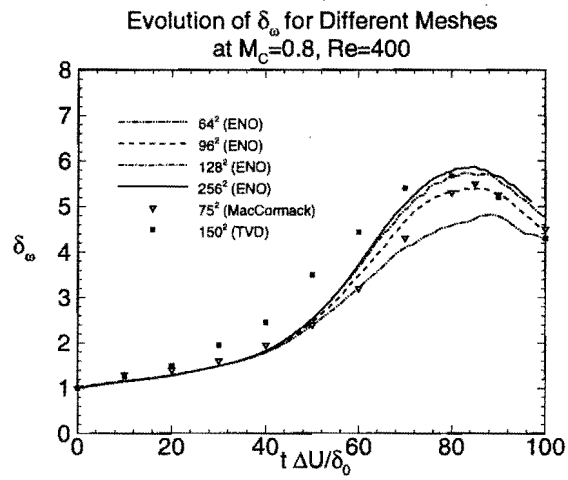

Fig. 4 Evolution of the vorticity thickness δ_ω at M_c = 0.8, Re = 400 for different meshes: present work (lines), Sandham and Yee (1989) (symbols)

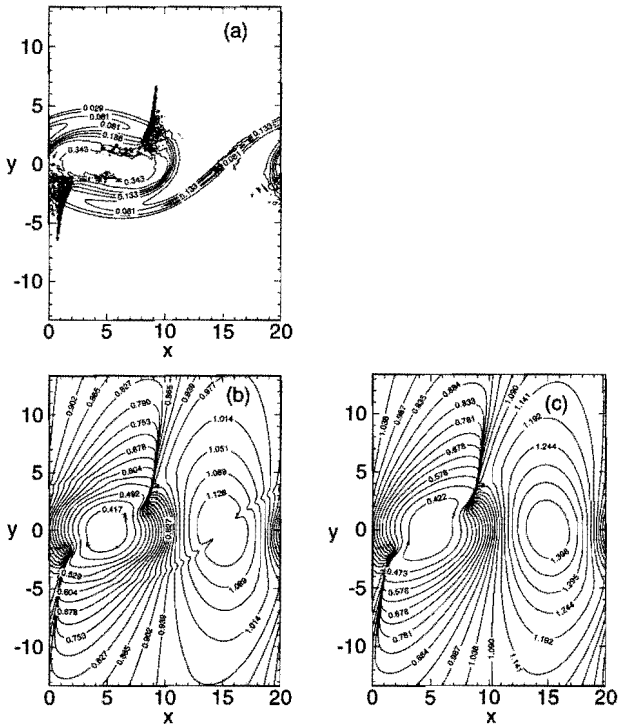

Fig. 5 Contour maps from the present work: (*a*) vorticity field, (*b*) density field, and (c) pressure field

shown in Fig. 5, which shows identical distribution to those reported by Sandham and Yee (1989) (not shown). The vortex rollup can be observed, as can the precision with which the local shock is captured. Some comments are in order for the oscillations in the density field of Fig. 5(*b*) as there exists at least two reasons to suggest why the oscillations might be physical. First, our numerical procedure is constructed to avoid such oscillations that are numerical in nature (Shu et al., 1989). For another, we have not observed the same oscillation with the pressure distribution (Fig. 5(*c*)), which on the basis of the similarity of the two fields, evidently requires the same computational challenge as the density field calculation.

It is important that numerical procedures be able to exhibit grid independence, if the results they provide are to be of any use. Grid independence of our code was investigated for the case M_c = 0.8, Re = 400 (see Fig. 4). The asymptotic behavior of our calculation can be observed: the curves become closer together as the grid is refined, such that the results are almost identical for 128^2 and 256^2. This kind of result generates confidence in the calculations. The results with MacCormack (75^2 mesh) and TVD (150^2 mesh) methods, which were carried out by Sandham and Yee (1989), are also presented in the same figure.

Our computer program has also been put through an accuracy study to determine the actual spatial accuracy of the schemes. The same grids shown in Fig. 4 are used for this study, whereby errors are measured assuming the results for 256^2 are "exact." The procedure for obtaining accuracy consists of the assumption that the error, E_i, for a grid denoted by "i," can be written as $E_i = \alpha \cdot \Delta_i^\beta$, where the further assumption is made that the constants α and β are the same for all grids. This error is defined as

$$E_i \equiv \overline{\delta}_{256} - \overline{\delta}_i,$$

where

$$\overline{\delta}_i \equiv \frac{1}{t}\int_0^t \delta_\omega^i \cdot dt,$$

which is a time-average of the vorticity thickness δ_ω. The con-

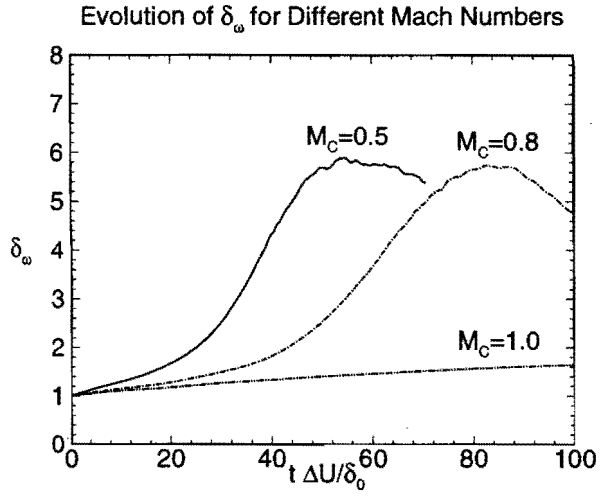

Fig. 6 Evolution of vorticity thickness δ_ω for different Mach numbers

stants α and β are determined using 64^2, 96^2, and 128^2 grid, via the least-square method. The result is

$$E_i \simeq 176.42 \cdot \Delta_i^{3.24},$$

which shows that the order of accuracy of our 2D ENO code is approximately third (Δ_i^3).

The validated computer program has been used to generate the mixing layer results shown in Figs. 6 through 10. Figure 6

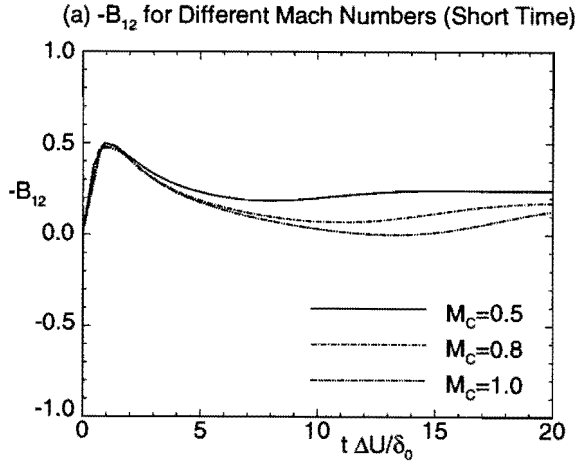

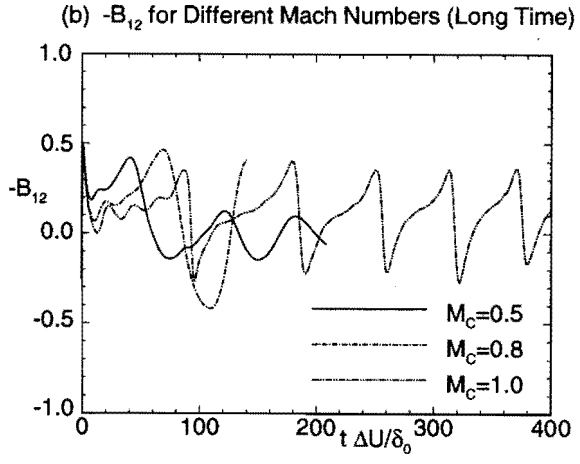

Fig. 7 Evolution of $-B_{12}$ for different Mach numbers: (a) short time, (b) long time

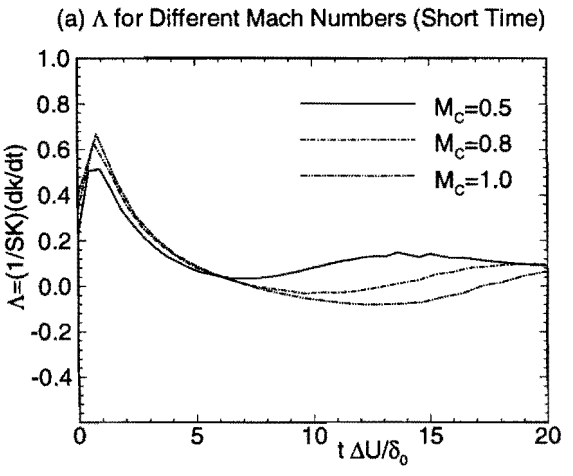

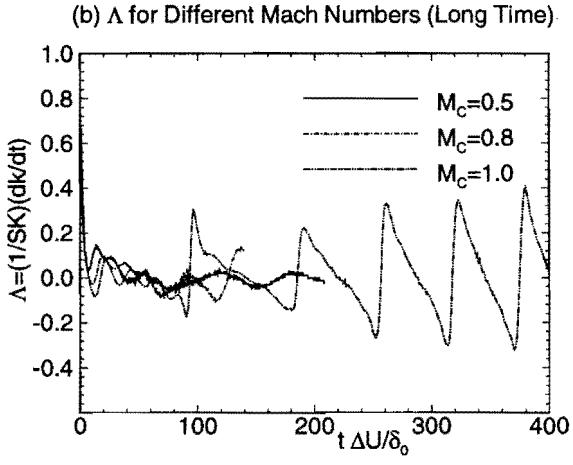

Fig. 8 Evolution of $\Lambda = (1/SK)(dK/dt)$ for different Mach numbers: (a) short time, (b) long time

shows the vorticity thickness (δ_ω) for three Mach numbers 0.5, 0.8 and 1.0 using the initial conditions described earlier in this paper. The Reynolds number is 400 for all cases. The well-known result of thinner layer thickness with increasing Mach number is reproduced in our calculation. In general, we observe an initial period of slow, linear growth and a much faster nonlin-

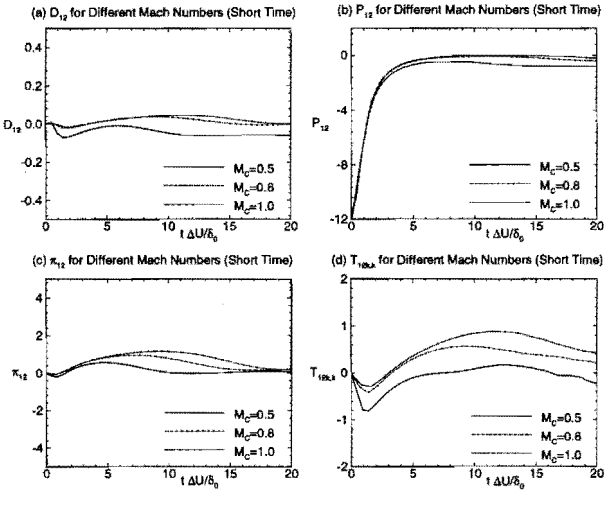

Fig. 9 Evolution of the "shear" components: (a) dissipation, D_{12}, (b) production, P_{12}, (c) pressure-strain, π_{12}, (d) transport, $T_{12k,k}$. Results are shown for short time.

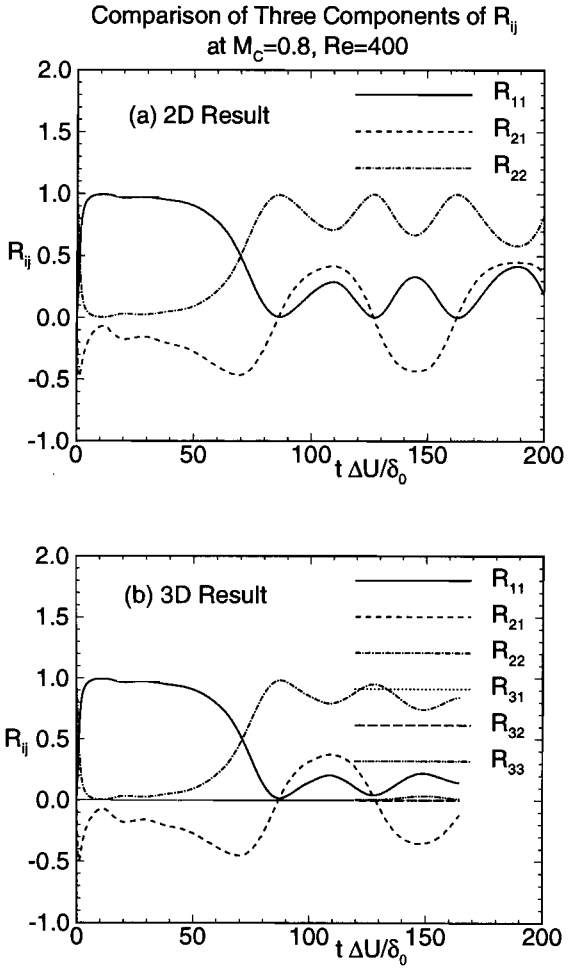

Fig. 10 Comparison of the components of Reynolds stress tensor $R_{ij} = \widetilde{u_i''u_j''}/2K$ for M_c = 0.8, Re = 400: (a) 2D results, (b) 3D results

ear growth at a later time, which are also consistent with those reported by Sandham and Reynolds (1991). For the case M_c = 0.5, no shocks were found in the flow field. However, for M_c = 0.8, local shock waves were generated during the development of vortex rollup. This phenomenon was also observed for the Mach numbers beyond 0.8.

A study of the evolution of the anisotropic tensor $B_{ij} = \widetilde{u_i''u_j''}/2K - (1/3)\delta_{ij}$ (here $K = (1/2)\widetilde{u_k''u_k''}$) shows that, at short time $0 < t' < 20$ ($t' = t \cdot \Delta U_\infty/\delta_0$), there is a systematic decrease in the quantity $-B_{12}$ with increasing Mach number (Fig. 7(a)). This might have already been implied by Sarkar (1995), who reported similar behavior for homogeneous shear flow. During the same time period, other quantities develop in a consistent pattern. The value of $\Lambda = (1/SK)(dK/dt)$, which describes the instantaneous temporal growth rate of K, tends to be higher for lower Mach numbers (Fig. 8(a)) (S is the shear rate, here defined as $S = (\partial\bar{u}/\partial y)_{y=0}$). Note that these results are consistent with those reported for homogeneous shear flow by Sarkar (1995), despite the differences in the initial conditions and problem setup. However, we observed that, at long time in the case of mixing layers, the behaviors do not show any consistent pattern. Each quantity shows a wavy evolution pattern, with larger amplitudes for increasing Mach number. The "shear" component B_{12} seems to approach a zero mean value at long time, although the oscillation is stronger for the higher Mach number cases (Fig. 7(b)). Similar observations were made for Λ (Fig. 8(b)).

Other terms in the Reynolds stress transport equation (3) are also studied. The magnitude of pressure-dilatation ($p'\theta$), as well as terms 2, Remaining Term1 and Remaining Term2 in (3) are all insignificant for all Mach number cases. Discussed here are the "shear" components of four tensors including dissipation (D_{ij}), production (P_{ij}), pressure-strain (π_{ij}), and transport ($T_{ijk,k}$). For convenience, these quantities are rescaled by SK with S and K defined as above. At short time, all four quantities (D_{12}, P_{12}, π_{12} and $T_{12k,k}$) show a similar variation with Mach number. That is, their magnitudes increase with increasing Mach number (Fig. 9(a), (b), (c) and (d)). The comparison of the three components of the Reynolds stress tensor $R_{ij} = \widetilde{u_i''u_j''}/2K$ for M_c = 0.8, Re = 400 shows that the R_{11} component dominates at early time, after which it decreases in magnitude and begins to oscillate. The other components, R_{12} and R_{22}, are significant in magnitude at later time, although with a large oscillation. R_{12} is negative for most of the time while other components are positive (Fig. 10(a)).

5 Discussion

It can be observed from our procedure that extra efforts were made to produce high quality calculations and to characterize the effective accuracy of our numerical procedures, which was found to be approximately $O(\Delta^3)$. Based on the grid convergence study, as well as some elementary scaling analysis (not shown), it would seem that the 128^2 grid is sufficient to resolve the necessary DNS scales, although most of the results have been generated with 256^2 grid. Evidently, higher parameter values may dictate different grid requirements.

The first interesting observation from the present study is the similar profile at early time for the kinetic energy growth rate Λ and the anisotropy tensor B_{ij} with quantities reported by Sarkar (1995) for the homogeneous shear flow. Initial and boundary conditions are different for these two problems so that, on the surface, there are few reasons to expect similar results. It would seem that the nature of shear and the definitions of these two quantities (Λ and B_{ij}) are such as to nullify the effects of initial and boundary conditions. However, at long time, when nonlinearity is stronger, the behaviors in the case of mixing layers show no consistent pattern. The literature does not report on the long time behavior in the homogeneous shear layer case, so that no comparisons can be made.

Although the calculations presented in this paper are two-dimensional, they might still be relevant to the physical engineering problem which is evidently three-dimensional (Moser and Rogers, 1993). To support this suggestion, we carried out a preliminary calculation of several three-dimensional mixing layers and compared some of the fields with the two-dimensional results, using similar initial conditions. For example, Fig. 10(b) is the Reynolds stress tensor obtained from the three-dimensional case. The short-time behavior clearly shows some agreement with the two-dimensional case. We point out that the two-dimensional initial conditions may not be appropriate for the three-dimensional simulations, from a mode excitation stand point. However, it is still true that the oblique shock waves, which are the optimal initial perturbation for the three-dimensional case, may not represent the physical engineering mixing layers. Thus, the comparison just discussed for two-dimensional and three-dimensional cases might be relevant.

The temporal oscillations in R_{ij} (Fig. 10(a)), as well as in Λ and B_{ij}, after the initial transient seems to be related to the vortex structure in the physical, spatial mixing layers. Equivalence between the temporal and physical mixing layers is assumed via the Taylor's hypothesis, which, for our setup, takes the form:

$$2\frac{\partial}{\partial t_e} = U_\infty \frac{\partial}{\partial x}$$

where $t_e = (\Delta U_\infty/\delta_0)t'$, with t' as the dimensional time.

Taking the case $M_c = 0.8$ as an example (Fig. 10(a)), the period of the oscillation of R_{11} is approximately 40 along the t_e axis, which corresponds to a traveling distance of 20 in space ($U_\infty = 1$). The latter is also equal to the size of our computational domain in which only one vortex is contained. Therefore, the temporal oscillations in some of these variables are related to the repetition of the domain under the assumption of periodicity in space.

To examine the validity of this explanation, we carried out a test in which two vortices were forced into the same size of computational domain. We observed that the flow contains two cells (not shown) at short time ($0 < t_e < 50$), but that the two cells coalesced into a single cell at a later time ($t_e > 100$). At short time, when two cells were present, the period of the oscillations reduced to approximately 20 in time t_e, corresponding to a streamwise spatial distance of 10, which is consistent with Taylor's hypothesis. When the two cells coalesced, the period in time t_e becomes 40, which is the same as that for the regular calculations with one vortex. Therefore, the explanation put forward above appears tenable.

Finally, the relevance of the second moment calculations to engineering may not be obvious. However, the results in this paper do show that, because of small magnitudes, modeling efforts do not need to place much emphasis on the pressure dilatation, the convective transport of Reynolds stress by the mean flow, the term $\boxed{2}$ and the "remaining" terms in Eq. (3). Specific numerical details of the various second moment terms are useful in order-of-magnitude analysis for turbulence model development. For example, models must recognize that R_{12} is negative, for applications within the ranges of the parameters reported in this paper. The reader may also appreciate that the temporal histories provided for the various turbulence quantities in Figs. (7) through (10) are, in fact, statements about the variation of these quantities along the streamwise direction. Obviously, this is useful turbulence model data.

Acknowledgments

This work was supported by the National Science Foundation under grant no. CTS 9626413, which we gratefully acknowledge.

References

Drummond, J. P., 1988, "A Two-Dimensional Numerical Simulation of a Supersonic, Chemically Reacting Mixing Layer," NASA TM 4055, Langley Research Center, Hampton, VA.

Ghosh, S., and Matthaeus, W. H., 1992, "Low Mach Number Two-Dimensional Hydrodynamic Turbulence: Energy Budgets and Density Fluctuations in a Polytropic Fluid," *Physics of Fluids,* Vol. A4, No. 1, pp. 148–164.

Ladeinde, F., 1995, "Supersonic Flux-Split Procedure for Second Moments of Turbulence," *AIAA Journal,* Vol. 33, No. 7, pp. 1185–1195.

Ladeinde, F., O'Brien, E. E., and Cai, X. D., 1996, "A Parallelized ENO Procedure for Direct Numerical Simulation of Compressible Turbulence," *Journal of Scientific Computing,* Vol. 11, No. 3, pp. 215–241.

Ladeinde, F., O'Brien, E. E., Cai, X., and Liu, W., 1995, "Advection by Polytropic Compressible Turbulence," *Physics of Fluids,* Vol. 7, No. 11, pp. 2848–2857.

Lee, S., Lele, S. K., and Moin, P., 1991, "Eddy Shocklets in Decaying Compressible Turbulence," *Physics of Fluids,* Vol. A3, No. 4, pp. 657–664.

Moser, R. D., and Rogers, M. M., 1993, "The Three-Dimensional Evolution of a Plane Mixing Layer: Pairing and Transition to Turbulence," *Journal of Fluid Mechanics,* Vol. 247, pp. 275–320.

Poinsot, T. J., and Lele, S. K., 1992, "Boundary Conditions for Direct Simulations of Compressible Viscous Flows," *Journal of Computational Physics,* Vol. 101, pp. 104–129.

Sandham, N. D., and Reynolds, W. C., 1991, "Three-Dimensional Simulations of Large Eddies in the Compressible Mixing Layer," *Journal of Fluid Mechanics,* Vol. 224, pp. 133–158.

Sandham, N. D., and Yee, H. C., 1989, "A Numerical Study of a Class of TVD Schemes for Compressible Mixing Layers," NASA TM 102194, Ames Research Center, Moffett Field, CA.

Sarkar, S., 1995, "The Stabilizing Effect of Compressibility in Turbulent Shear Flow," *Journal of Fluid Mechanics,* Vol. 282, pp. 163–186.

Sarkar, S., Erlebacher, G., Hussaini, M. Y., and Kreiss, H. O., 1991, "The Analysis and Modelling of Dilatational Terms in Compressible Turbulence," *Journal of Fluid Mechanics,* Vol. 227, pp. 473–493.

Shu, C.-W., and Osher, S., 1989, "Efficient Implementation of Essentially Non-Oscillatory Shock Capturing Schemes II," *Journal of Computational Physics,* Vol. 83, pp. 32–78.